International Journal of Innovative Computing, Information and Control
Volume **9**, Number **5**, May **2013**

 ISSN 1349-4198
pp. 1835–1850

AN INNOVATIVE APPROACH FOR DETECTION OF SLIGHT SURFACE VARIATIONS ON CAPACITOR CHIPS

Hong-Dar Lin[1,*], Yuan-Shyi Peter Chiu[1] and Wan-Ting Lin[2]

[1]Department of Industrial Engineering and Management
Chaoyang University of Technology
168 Jifong E. Rd., Wufong District, Taichung 41349, Taiwan
*Corresponding author: hdlin@cyut.edu.tw

[2]Department of Marketing
University of Texas at San Antonio
One UTSA Circle, San Antonio, TX 78249, USA

Received February 2012; revised June 2012

Abstract. *This paper presents an innovative approach to develop a machine vision-based quality inspection system for surface variation detection on passive components. The developed system applies discrete cosine transform (DCT) based image reconstruction method for automated detection of slight surface variations on capacitor chips. We first perform the DCT transformation to transform a spatial domain image into the frequency domain. From the energy concentration analysis of the DCT domain, we can disassemble the frequency matrix into four disassembled matrices. We select the proper number of larger frequency values to represent the random structure features of the capacitor chip surface from the disassembled matrices. Then, we set the selected frequency values to zero and reconstruct the image. For a defective capacitor chip, the slight surface variations will be reserved and the random patterns will be eliminated in the restored image. Finally, the entropy method is applied to setting a threshold for distinguishing between slight surface variation regions and uniform regions in the restored image. Experimental results show that the proposed method achieves a high 96.66% probability of correctly discriminating slight surface variations from normal regions and a low 0.12% probability of erroneously detecting normal regions as slight variations on random textured surfaces of capacitor chips.*

Keywords: Slight surface variation, Capacitor chips, DCT disassembly, Entropy, Machine vision

1. **Introduction.** Passive components (e.g., resistors, capacitors and inductors) contribute no power amplification in the circuit system and require only a signal to start their functions. As passive components require low or no power consumption, their importance and popularity have been increasing in these years when energy conservation issues intensify. The number of passive components used in Printed Circuit Boards (PCBs) has grown to a large extent in much smaller electronic products. More than 80% of the parts in a motherboard are composed of passive components. With the popularity of passive components, inspection of surface variations has become a critical task for manufacturers who strive to improve product quality and production efficiency of passive components. To contribute to the field of surface variation inspection on passive components, this research uses round Surface Barrier Layer (SBL) chips as testing samples. SBL chips are passive components (ceramics capacitors) commonly used in many electronic appliances.

Surface variations affect not only the appearance of electronic devices but also their functionality, efficiency and stability. Large and obvious surface variations such as indents, scraps and scratches are usually inspected by automated visual inspection systems.

However, slight surface variations such as dust, cavities and pinholes are very difficult to detect because of their extremely small sizes. Nevertheless, it is also hard to precisely inspect slight surface variations by machine vision systems. When product images are being captured, the area of a slight surface variation could expand, shrink or even disappear due to the uneven illumination of the environment, complex texture of the product surface, and so on. Thus, the inspection accuracy of the machine vision system is greatly reduced. To overcome the difficulties of detecting slight surface variations, this paper presents a machine vision-based quality inspection system to automatically detect the slight surface variations on ceramic capacitor chips.

Although slight surface variations occupy only small areas on the product surface, they could affect the appearance, functions and security of the product. With a width of 0.005 mm and a diameter of 7 mm, the capacitor chips are small in size, light in weight, and suitable for mass and large-lot-sized production. Figure 1 shows (a) a capacitor chip carrier plate used in the manufacturing process, (b) faultless and defective capacitor chips, and (c) a chip image without any slight surface variation. Slight surface variations often appear on the surfaces of capacitor chips and occupy only extremely small areas. For an capacitor chip image of 256×256 pixels, the size of its slight surface variation falls within the range of $1 \sim 15$ pixels and occupies $0.0015\% \sim 0.0229\%$ of the image area. Surface defects of this magnitude are defined as slight surface variations in this research. Figure 2 shows capacitor chips with slight surface variations of different shapes. Aiming to improve the inspection accuracy of slight surface variations, this research proposes a Discrete Cosine Transform (DCT) based enhancement approach to overcome the difficulties of traditional machine vision systems in detecting slight surface variations.

This research presents a global approach for the automated visual inspection of slight surface variations on capacitor chip surfaces. As common machine vision systems are not good at detecting slight surface variations, we transform a digital image to DCT domain and analyze the energy trends of the frequency matrix. After some frequency components

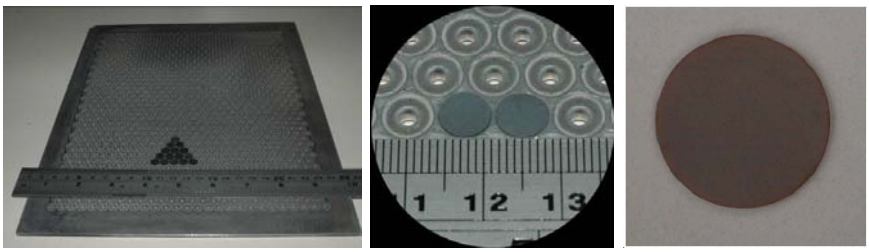

(a) (b) (c)

FIGURE 1. (a) A capacitor chip carrier plate; (b) faultless and defective capacitor chips; (c) a capacitor chip without any slight surface variation

FIGURE 2. Capacitor chips with slight surface variations of different shapes

of the normal regions are removed, the rest of the components are transformed back to spatial domain to produce a restored image with enhanced slight surface variations. These enhanced slight surface variations can be easily separated from the normal regions by an entropy method.

2. **Surface Variation Detections.** Assessment of surface blemishes of industrial products has become a critical task for manufacturers who strive to improve product quality and production efficiency [1]. Blemish detection techniques, generally classified into the spatial domain and the frequency domain, compute a set of textural features in a sliding window and search for significant local deviations among the feature values. Recently, an automatic vision defect inspection system has been proposed for detecting defects on highly specular reflection curved surfaces by using image reconstruction, morphological technique, and template matching. Zhang et al. [2] applied template matching using morphological processing to detect defects on metal plating surfaces. Chang et al. [3] presented a new approach for inspecting LED wafer defects using Learning Vector Quantization (LVQ) neural networks. Araki et al. [4] used independent component analysis to detect blemishes for mirror polished metal surfaces.

Fourier transform, wavelet transform and Gabor transform are common texture analysis techniques used in the frequency domain. Li and Tsai [5] demonstrated a blemish detection method based on image reconstruction of Fourier transform and Hough-like nonstationary line detection to identify saw-mark blemishes in multicrystalline solar wafer images. Han and Shi [6] proposed an adaptive level-selection approach based on wavelet transform to detect defects on images with high frequency texture background. Lin [7] used the one-level Haar wavelet transform to decompose color images of surface barrier layer chips and extracted wavelet features from normal samples and testing samples were statistically compared based on Hotelling, Mahalanobis, and Chi-square distances to identify ripple blemishes on the chip images. Liu et al. [8] presented two methods of designing Gabor filters for extracting slub in both the time domain and the frequency domain. The first method selects a better filter in the time domain according to a designed cost function. The second method obtains the proper parameters for the filter in the frequency domain according to the frequency characteristic of slubs. Also, Lin and Chiu [9] proposed a machine-vision-based system that applies block discrete cosine transform and grey relational analysis for the automated visual inspection of tiny flaws occurred in the domed surfaces of LED epoxy-packing. Kumar [10] and Ngan et al. [11] surveyed and reviewed the articles related to fabric defect detection methods published in the last decades. These machine vision-based techniques were summarized, classified, and commented in a comparison manner.

Use of the DCT in a wide variety of applications has not been as extensive as its properties would imply due to the lack of an efficient algorithm. Thus, many algorithms and VLSI architectures for the fast computation of DCT have been proposed [12-14]. Chen et al. [15] developed new and fast algorithms for edge enhancement of remote sensing image data in the DCT domain and implemented in three steps: high-pass filtering, adding back full or part of gray levels to the original image, and contrast stretching. Zhong and Jain [16] proposed an algorithm for object localization using shape, color, and texture. The texture and color features are directly extracted from the DCT compressed domain and are used to find a small number of candidate images in the database, and regions in the candidate images which share similar texture and color as the query can be identified. Ngo et al. [17] presented approaches for indexing shape, texture, and color features directly in the DCT domain by exploiting ten DCT coefficients. Overall, the retrieval results are competent since most of the top retrieved images are relevant.

3. **Proposed Methods.** We first perform the DCT transformation to transform a spatial domain image into the frequency domain. From the energy concentration analysis of the DCT domain, we can disassemble the frequency matrix into four disassembled matrices. We select the proper number of larger frequency values to represent the random structure features of the capacitor chip surface. Then, we set the selected frequency values to zero and reconstruct the image. Finally, the entropy method is applied to set the threshold for distinguishing between slight surface variation regions and uniform regions in the restored image.

3.1. **DCT frequency domain analyses.** Since digital images are two dimensional discrete data arrays, two dimensional DCT transform is needed to process the transformation. The DCT of an image $d_{x,y}$ of size $M \times N$ is given by the Equation (1) [18]. This expression must be computed for values of $u = 0, 1, 2, \ldots, M-1$, and also for $v = 0, 1, 2, \ldots, N-1$. Similarly, given $D_{u,v}$, we obtain $d_{x,y}$ via the inverse DCT transform, given by the Equation (2) for $x = 0, 1, 2, \ldots, M-1$ and $y = 0, 1, 2, \ldots, N-1$. Equations (1) and (2) comprise the two-dimensional, DCT pair. The variables u and v are frequency variables, and x and y are spatial variables.

$$D_{u,v} = \rho(u)\rho(v) \sum_{x=0}^{M-1} \sum_{y=0}^{N-1} d_{x,y} \cos\left[\frac{(2x+1)u\pi}{2M}\right] \cos\left[\frac{(2y+1)v\pi}{2N}\right] \tag{1}$$

$$d_{x,y} = \sum_{u=0}^{M-1} \sum_{v=0}^{N-1} \rho(u)\rho(v) D_{u,v} \cos\left[\frac{(2x+1)u\pi}{2M}\right] \cos\left[\frac{(2y+1)v\pi}{2N}\right] \tag{2}$$

where

$$\rho(u) = \begin{cases} \sqrt{\frac{1}{M}}, & u = 0 \\ \sqrt{\frac{2}{M}}, & u = 1, 2, 3 \ldots, M-1 \end{cases},$$

$$\rho(v) = \begin{cases} \sqrt{\frac{1}{N}}, & v = 0 \\ \sqrt{\frac{2}{N}}, & v = 1, 2, 3, \ldots, N-1 \end{cases},$$

$$\begin{cases} u = 0, 1, 2, \ldots, M-1 \\ v = 0, 1, 2, \ldots, N-1 \\ x = 0, 1, 2, \ldots, M-1 \\ y = 0, 1, 2, \ldots, N-1 \end{cases}.$$

The power spectrum $P(u, v)$ of image $d_{x,y}$ is defined as:

$$P(u, v) = |D_{u,v}|^2 \tag{3}$$

That is, the energy of the image can be obtained by adding up the squares of the DCT coefficients.

As the origin of the DCT coefficients has a very huge frequency value, it is sometimes called the Direct Current (DC) component of the spectrum, while other coefficients are called the Alternating Current (AC) components. The DC coefficients in the upper left corner reflect information of lower frequencies, whereas the AC coefficients in the lower right corner reflect that of higher frequencies. The high-pass filter attenuates low frequencies and passes high frequencies. A high-pass filtered image is sharper than the original image because the low frequencies have been attenuated. Based on the DCT filtering property, we can obtain a restored image with enhanced transitional gray level details, if we apply a high-pass filtering operation in the frequency domain and then perform an inverse DCT.

The 3-D DCT spectrum diagram in Figure 3(a) shows that a lot of energy concentrates in the origin ($u = 0$, $v = 0$) and that the energy decreases gradually from the origin and the low frequency zone to the high frequency zone. Based on the fluctuations of the frequency trend and the properties of the low and high frequency zones, we design a high-pass sector filter centered at the origin of the 2-D DCT spectrum to filter out major low frequency components of the spectrum image. An adequate radius is first determined for the sector filter in the spectrum space. Frequency components (low frequencies) within the radius of the sector filter are then set to zero, and those outside the filter (medium and high frequencies) are retained. Finally, the inverse DCT is applied to transform the filtered image back to the spatial domain. Figure 3(b) demonstrates a 3-D DCT spectrum diagram with a high-pass sector filter.

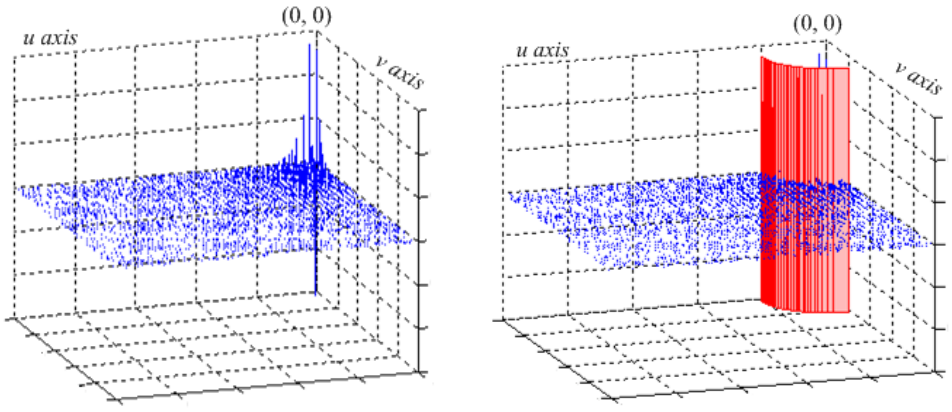

(a) (b)

FIGURE 3. A high-pass sector filter added into a 3-D DCT spectrum diagram: (a) A 3-D diagram of a DCT spectrum; (b) A 3-D diagram of a DCT spectrum with a cutting sector radius

The low frequency components with larger magnitude represent the global approximation of the original image. All other middle and high frequency components provide the local, detailed information of the image [14]. Therefore, we can select a proper radius for the frequency components of larger magnitude to represent the global, repetitive textural feature of the image and remove such background texture by reconstructing the image without the use of larger-magnitude frequency components. In the following subsections, we propose a DCT disassembly and cumulative sum analysis procedure to automatically determine an appropriate sector radius for image restoration.

3.2. **Disassembly of DCT domain.** As given in Equation (1), $D_{u,v}^{\#1}$ is the discrete cosine transform of a testing image $d_{x,y}^{\#1}$ of size $M \times N$. Let G^* be a waveform sign of 1-D frequency arrays and axis be a 1-D coordinate vector. Then, $G^*(axis)$ is a waveform plot along the axis coordinate and can be denoted as:

$$G^*\left(axis\right) = D_{u,v}^{\#1} \tag{4}$$

where $axis = D_{u,0\sim(N-1)}^{\#1}$ or $D_{0\sim(M-1),v}^{\#1}$; $u = 0, 1, 2, \ldots, M-1$; $v = 0, 1, 2, \ldots, N-1$. Figure 4 shows the plots of 1-D waveform arrays $G^*(D_{0\sim(M-1),v}^{\#1})$ of a DCT frequency matrix along the u axis and demonstrates that the waveforms of the $G^*(D_{0\sim(M-1),v}^{\#1})$ remain stable until they approach the DC location. And, the closer the waveforms are to the DC location,

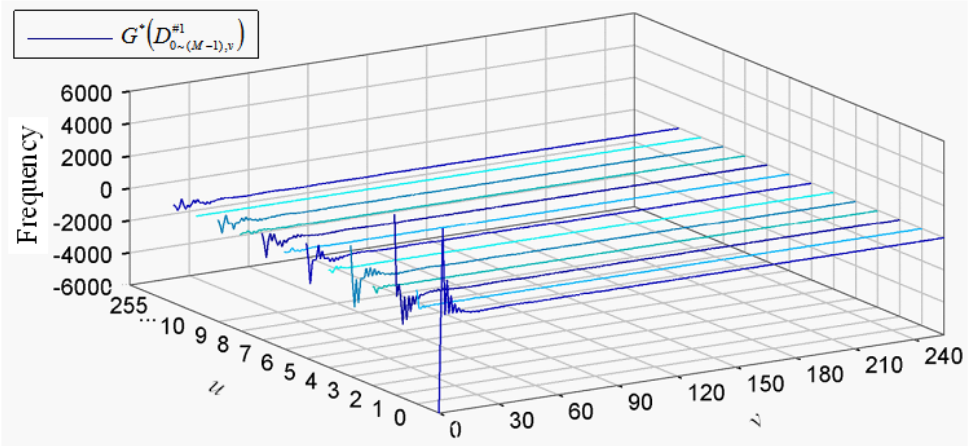

FIGURE 4. 1-D waveform plots $G^*(D^{\#1}_{0\sim(M-1),v})$

the more widely they fluctuate. The magnitude of frequency components that are far away from the top left origin in the DCT domain falls rapidly and approximates zero.

We disassemble the 2-D DCT domain $D^{\#1}_{u,v}$ into two matrices: the odd matrix $DO_{u,v'}$ and the even matrix $DE_{u,v'}$, whose definitions are given below:

$$DO_{u,v'} = D^{\#1}_{u,2v'} \tag{5}$$

$$DE_{u,v'} = D^{\#1}_{u,2v'+1} \tag{6}$$

where $u = 0, 1, 2, \ldots, M-1$; $v' = 0, 1, 2, \ldots, (N/2)-1$. The odd-number frequencies of the v axis form the odd frequency matrix $DO_{u,v'}$, while the even-number frequencies make up the even frequency matrix $DE_{u,v'}$. The v' axis in either the odd or the even frequency matrix is half as long as the v axis in the original frequency matrix $D^{\#1}_{u,v}$. Therefore, the original frequency matrix $D^{\#1}_{u,v}$ can be further disassembled into odd-odd $DOO_{u',v'}$, odd-even $DOE_{u',v'}$, even-odd $DEO_{u',v'}$, and even-even $DEE_{u',v'}$ matrices under the alternating decomposition of odd and even parts. These four matrices can be denoted as follows, respectively:

$$DOO_{u',v'} = D^{\#1}_{2u',2v'} \tag{7}$$

$$DOE_{u',v'} = D^{\#1}_{2u',2v'+1} \tag{8}$$

$$DEO_{u',v'} = D^{\#1}_{2u'+1,2v'} \tag{9}$$

$$DEE_{u',v'} = D^{\#1}_{2u'+1,2v'+1} \tag{10}$$

where $u' = 0, 1, 2, \ldots, (M/2)-1$; $v' = 0, 1, 2, \ldots, (N/2)-1$.

After the original frequency matrix $D^{\#1}_{u,v}$ is disassembled into four matrices (Equations (7) to (10)), we can use the G^* waveform plot to examine the frequency fluctuations of the waveform matrices. Since each frequency matrix has two dimensions, u' and v' axes, the four disassembled frequency matrices will have eight sets of 1-D waveform arrays. To obtain the right sector radii that help improve the analysis results, the negative 45 degree diagonal coefficients of the frequency matrix can be disassembled into a 1-D array DA_t when M and N are equal and the top left DC location is set as the origin. This diagonal matrix can be denoted as follows:

$$DA_t = D^{\#1}_{t,t} \tag{11}$$

where $t = 0, 1, 2, \ldots, M-1$.

The frequencies of the waveform plot $G^*(DA_t)$ of the matrix DA_t fluctuate in the same way as those of the waveform matrices $G^*(DO_{0\sim(M-1),v'})$ and $G^*(DE_{0\sim(M-1),v'})$. Thus,

we can further disassemble the matrix DA_t into $DAO_{t'}$ and $DAE_{t'}$ matrices. These two matrices can be denoted as follows:

$$DAO_{t'} = DA_{2t'} \tag{12}$$

$$DAE_{t'} = DA_{2t'+1} \tag{13}$$

where $t' = 0, 1, 2, \ldots, (M/2) - 1$. After completing the disassembly procedure, we examine the frequency fluctuation trends of the waveform plots G^* of the four disassembled frequency matrices (Equations (7) $\sim$ (10)). We find that the waveform plots of the 1-D odd arrays show significant and systematic frequency changes. The frequency fluctuation trends of the odd-odd matrix are smoother and more predictable when compared with those of the other disassemble matrices. The DCT frequency matrix $D^{\#1}_{u,v}$ needs to be disassembled because most of the regular waveform plots come from the disassemble odd-odd matrix $DOO_{u',v'}$. Therefore, the odd-odd frequency matrix $DOO_{u',v'}$ (including the diagonal matrix $DAO_{t'}$) will be the main target of the later analyses.

3.3. **Cumulative sum (CUSUM) control scheme for radius selection.** To select the proper sector radius, we propose a transition point detection method that uses the DC location as the origin of the sector area to locate the low-frequency regions. The proper radius R^* of the sector area is determined at the point where the frequency fluctuation trend gets stable. A stable frequency trend signifies that the frequencies are no longer in the low-frequency regions. Similar to the waveform plots $G^*(axis)$ of the disassembled frequency matrices, the waveform plots of the disassembled odd-odd matrix $DOO_{u',v'}$ perform better in detecting the transition point when the frequency trend turns stable. Therefore, this research analyzes three sets of frequency arrays $DOO_{u',0}$, $DOO_{0,v'}$, and $DAO_{t'}$ to determine the proper radius R^* of the sector.

To detect the transition points in the gentle curves, this research proposes the CUSUM algorithm, which is commonly used in statistical process control to detect the slight shift or deviation from the normal production process [19]. Generally, the CUSUM method processes data, that are smooth in the beginning periods and that deviate slightly in the later periods. However, since the curves fluctuate sharply in the beginning periods and then turn smooth in the other periods, our algorithm applies the reverse order CUSUM method, which processes data in the reverse direction.

Suppose that Z sample sets with sample size $n = 1$ are collected, and X_z is the observation of the z-th sample, where $z = 1, 2, 3, \ldots, s, \ldots, Z$. The cusum scheme works by accumulating derivations from μ_0 that are above target with one statistic C_s^+ and accumulating derivations from μ_0 that are below target with another statistic C_s^-. The statistics C_s^+ and C_s^-. are called one-sided upper and lower cusums, respectively. They are computed as follows [19]:

$$C_s^+ = \max\left[0, \;\; X_s - (\mu_0 + K) + C_{s-1}^+\right] \tag{14}$$

$$C_s^- = \max\left[0, \;\; (\mu_0 - K) - X_s + C_{s-1}^-\right] \tag{15}$$

where $C_0^+ = C_0^- = 0$, $K = \frac{\delta}{2}\sigma$.

In Equations (14) and (15), K is usually called the reference value, and it is often chosen about halfway between the target μ_0 and the out-of-control value of the mean μ_1 that we are interested in detecting quickly. Thus, if the shift is expressed in standard deviation units as $\mu_1 = \mu_0 + \delta\sigma$, then K is one-half the magnitude of the shift. Note that C_s^+ and C_s^- accumulate deviations from the target value μ_0 that are greater than K, with both quantities reset to zero on becoming negative. If either C_s^+ or C_s^- exceeds the decision interval H, the process is considered to be out-of-control. A reasonable value for H is four or five times the process standard deviation σ [19].

The data sequence should be arranged in a reverse order before the reverse-order CUSUM method is applied. According to the definitions of the CUSUM method (Equations (14) and (15)), we assume C_z^+ and C_z^- as the one-sided upper and lower cusums of the sequence X_z, respectively. We must substitute the data of the three disassembled frequency matrices $DOO_{u',0}$, $DOO_{0,v'}$, and $DAO_{t'}$ into the sequence X_z^*, respectively, before applying the proposed reverse-order CUSUM method. Then, from the situations of being within or beyond a decision interval H, we determine the status of the process variation and identify the transition points $P(DOO_{u',0})$, $P(DOO_{0,v'})$, and $P(DAO_{t'})$ of the three frequency matrices.

The first value in each of the three frequency matrices $DOO_{u',0}$, $DOO_{0,v'}$ and $DAO_{t'}$ is the DC value in a DCT domain. This value represents the average gray level of an image and is usually the extreme value (the largest or the smallest) in a frequency matrix. Hence, this research sets the DC value at zero when detecting the transition points in the gentle curves to determine the proper radius of the sector filter. Setting the DC value at zero will avoid significant variations among the frequency components. After the calculations in Equations (14) and (15), three transition points will be identified in the gentle curves by the R-CUSUM method. The proper radius of the sector filter R^* can be denoted as:

$$R^* = 2AVG(P_\alpha, P_\beta, P_\omega) + 1 \tag{16}$$

where $AVG(P_\alpha, P_\beta, P_\omega) = average(P_\alpha, P_\beta, \sqrt{2}P_\omega)$. The proper radius R^* is selected based on the average radius of the transition points of the gentle curves along the three principal frequency arrays in the disassembled odd-odd matrix.

The calculation of the proper radius R^* is presented in Equation (16), where three transition points are used. Figure 5 shows points P_α, P_β, and P_ω are the three transition points of the gentle curves along u', v', and diagonal axes, respectively. The point P_ω must be multiplied by a weight of $\sqrt{2}$ because this point comes from the diagonal matrix $DAO_{t'}$ and must be adjusted to be in the same scale as P_α and P_β. And then, the three transition points are substituted into Equation (16) to compute the best filter radius R^*.

If the cumulative deviation sums reveal the trend of cyclic accumulations, then it means the data of the sequence are auto-correlated [19]. Cyclic accumulations may increase the chances of making wrong detection judgments and picking the wrong transition points. To overcome the problems of cyclic accumulations, we propose the reverse order difference CUSUM method (RD-CUSUM), which is also based on the CUSUM scheme to detect transition points. However, the RD-CUSUM method reverses the data sequence of the frequency array and calculates the difference between two successive data before the CUSUM algorithm is implemented. The difference function $L(x_z^*)$ calculates the new reverse-order difference sequence $L(x_{z-1}^*)$ by subtracting the reverse-order value x_{z-2}^* in period $(z-2)$ from the reverse-order value x_{z-1}^* in period $(z-1)$. Through the calculation of the reverse-order difference sequence, we can eliminate the cyclic accumulation phenomenon in the cumulative deviation sums. Figure 6 shows the calculation of the best filter radius R^* by the RD-CUSUM method.

3.4. **Entropy method for blemish separation.** After the proper sector radius R^* is determined, the frequency filtering operation can accurately specify the non-defect low frequency regions and set the values of their frequencies at zero in the DCT domain. Thus, the filtered frequency image $D_{u,v}^{\#2}$ can be transformed back to the spatial domain to produce a corresponding restored image $d_{x,y}^{\#2}$ by using Equation (2). When a restored image with enhanced slight surface variations is generated, an automated thresholding technique called Kapur's entropy method [20] is applied to separate the slight surface variations from the normal regions. Figure 7 shows the whole process of the proposed

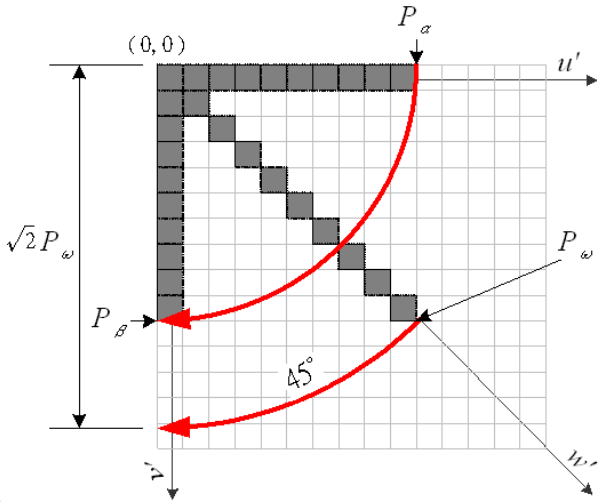

FIGURE 5. A sector radius diagram obtained from transformation of the three principal frequency arrays

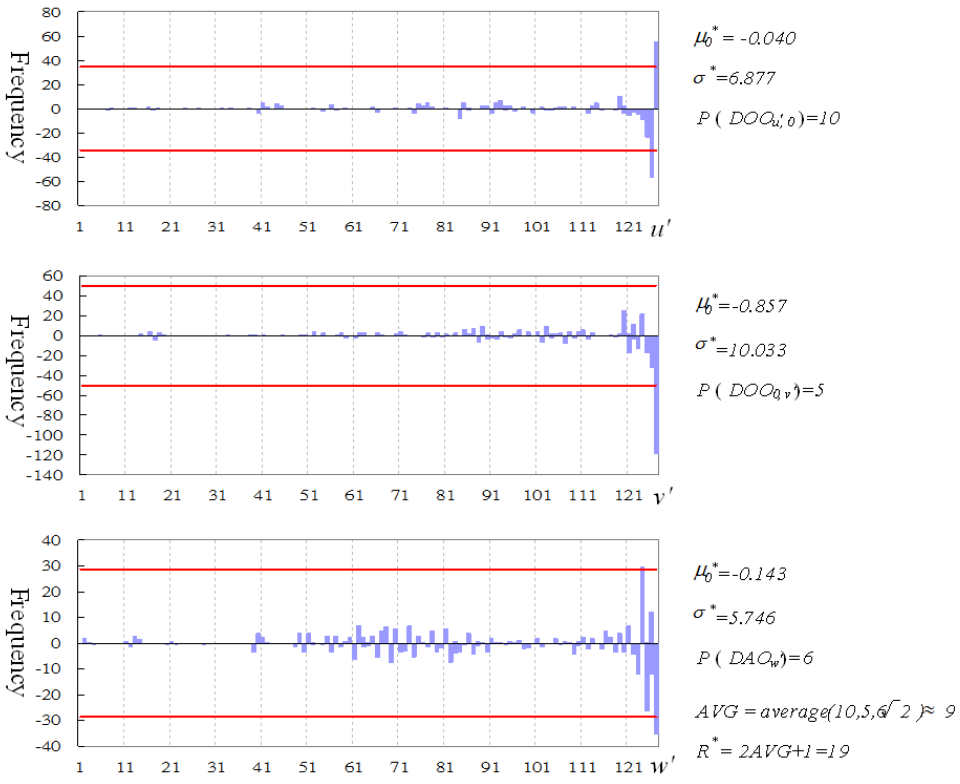

FIGURE 6. Calculation of the filter radius R^* by the RD-CUSUM method

DCT based enhancement approach for slight surface variation detection on capacitor chips. A testing image with slight surface variations which are difficult to detect in the spatial domain is processed by the proposed DCT high-pass filtering operation. Then, taking the inverse DCT of the filtered result, the surface variations can be segmented by the Kapur's entropy method.

Let an image with gray levels in the range $[0, L-1]$. We assume S_l be the number of pixels in the image having gray level l and the total number of pixels in the image should be $\sum_{l=0}^{L-1} S_l$. Then, Y_l is an estimate of the probability of occurrence of gray level l in the

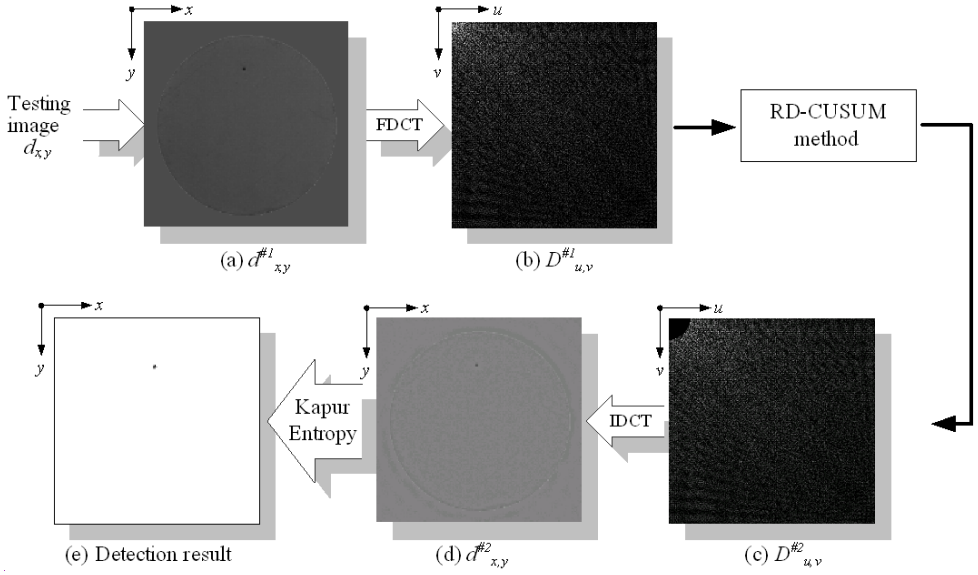

FIGURE 7. Procedures of the proposed approach for detecting slight surface variations on capacitor chip

image, denoted as $Y_l = S_l \Big/ \sum_{l=0}^{L-1} S_l$. From the definition of entropy, the entropy of an image is $N = -\sum_{l=0}^{L-1} Y_l \ln Y_l$. We aim to classify the pixels of the image into two opposite classes, namely flaw (black) and normal region (white) by thresholding. The entropy of the defective portion of an image is $N_O(T)$ and the entropy of the normal portion of an image is $N_B(T)$. Therefore, the Kapur's entropy method is to determine the value of the threshold T, such that the total entropy N (Equation (17)) of the partitioned image is maximized.

$$N = N_O(T) + N_B(T) = -\sum_{r=0}^{T} Y_r \ln Y_r - \sum_{r=T+1}^{L-1} Y_r \ln Y_r \tag{17}$$

The Kapur's entropy method outperforms many other methods in detecting small objects [21]. However, the entropy method cannot correctly separate slight surface variations if the chip image does not go through the defect enhancement step of the proposed DCT frequency filtering operation. This is because many noises in the image may incur erroneous judgment in flaw separation. If an image is processed by the proposed DCT-based image reconstruction approach in advance, the slight surface variations in the image can be precisely located by the Kapur's entropy method.

4. **Implementation and Analyses.** We make use of the following equipments: a white ring LED lighting device, a charge-coupled device (CCD) camera model WAT-221S of Watec company, a lens with 1 to 10 amplifications of changeable focal lengths, a frame grabber model IMAQ PCI-1411 of National Instruments corporation, and a XYZ electronic control table with a controller. Figure 8 shows the configurations of the experimental environment and hardware setup in which we scan real capacitor chips to be used as testing samples. Each image of the chip has a size of 256×256 pixels and a gray level of 8 bits. The 150 images are defective chips with one or more than one slight surface variations and the other 50 images are regular chips without any slight surface variation. The slight surface variation detection algorithm is edited and executed on the sixth version of C++ Builder complier on a personal computer (Pentium-4 2.8 GHz and 1GB DDRII 667 Hz-RAM).

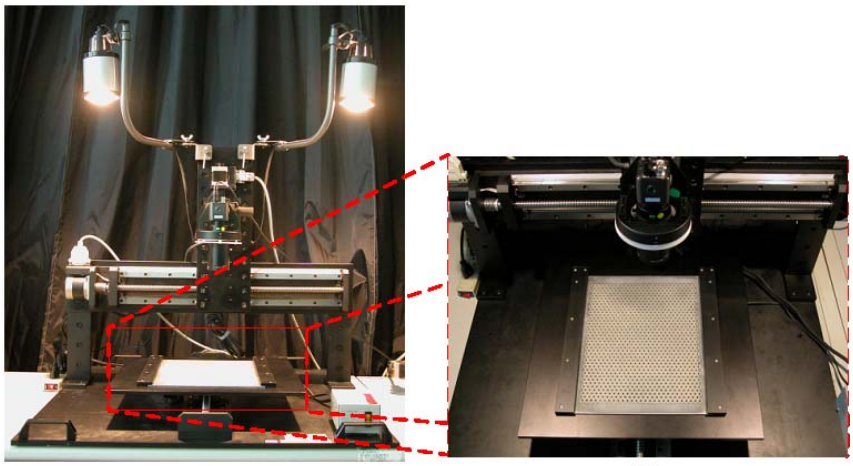

FIGURE 8. (a) Configurations of experimental environment; (b) hardware setup of the conducted experiments

4.1. **Pre-processing of DCT enhancement.** Region of interest (ROI) is a rectangle (block) that contains the object to be investigated. The use of ROI can avoid the interference of uninterested regions when mask computations or frequency transformations are conducted. If an image containing uninterested regions is transformed into the DCT domain, the uninterested region can significantly interfere in the frequency analysis of the ROI. Therefore, after we use CCD and XYZ electronic control table to acquire the image of the target chip and its six neighboring chip fragments, we produce a target mask to delineate the ROI, the region of the target chip. Then we obtain a mixed image by combining the target region with a manipulated background to decrease the interference of an uninterested region. This mixed image will then be used as the input for further DCT transformation.

To maximize the number of chips on the carrier plate, every chip is located very close to its neighboring chips. Thus, while the image of a specific chip is captured, the image covers not only the whole of the specific chip but also fragments of its six neighboring chips (as shown in Figure 9(a)). Thus, the images of all the chips might be captured with slight differences; that is, not all chips are located in the exactly same positions in their individual images. As a result, a target mask is needed for each image to specify the location of the target chip. Figure 9 presents the procedure for producing a target mask for a target capacitor chip.

In Figure 9, the testing image is first captured and input. Second, a cross is located right in the middle of the image (not the middle of the target chip), and the average gray level of the cross region is computed. Assuming the length and width of the cross region are each composed of Wd pixels, there will be (2 Wd - 1) pixels to be computed to get the average gray level, which is denoted as PA (PA is set at 20 in this research). Third, based on a predefined criterion a region growing procedure is applied to group pixels of similar gray levels into a larger region. This procedure starts from a seed point (the image center in this case) and searches for those neighboring pixels whose gray levels fall within the range $(PA \pm Tr)$, where Tr is the gray level tolerance. IR_1 is used to denote the region whose pixels have gray levels in the specified range. Fourth, on the surface of a capacitor chip exists some noise pixels, whose gray levels do not fall into the specified range but which are located within the IR_1 region. The new grown region is denoted as IR_2 and its complement set as IR_2'. Finally, we re-assign the region IR_2' as IR_m, which is the

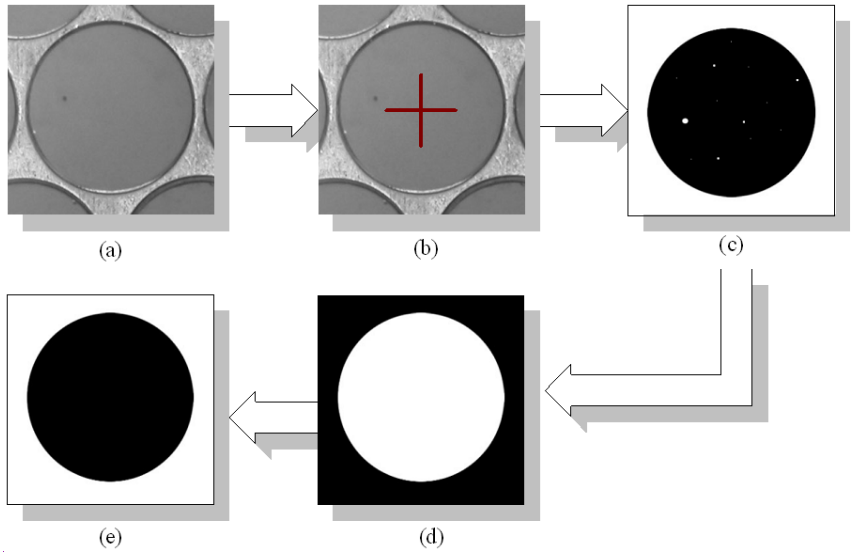

FIGURE 9. The procedure for producing a target mask for a target capacitor chip: (a) input a testing image; (b) calculate the average gray level of the central cross region; (c) compare and select the pixels whose gray levels in a specified range; (d) select the pixels whose gray levels in the same range as that of the top left corner pixel; (e) select the reverse region of the previous step to obtain a target mask

target mask of the testing image and which can specify the accurate region of the target capacitor chip.

In Figure 10, the original image (a) covers not only the whole of the target chip but also fragments of its six neighboring chips. In the target mask image (b), all non-target regions are removed, and the region of the target chip is delineated by the black circle after the target mask is applied. The clear silhouette of the target chip shows that the target mask has successfully performed its designated functions. In the mixed image (c), a manipulated background is formed by filling up all the non-target regions with the average gray level of the cross region in Figure 9(b). And, a mixing operation is done to integrate the foreground (the target region) with the manipulated background to obtain a rectangular ROI. As the foreground and the background are in similar gray levels now, we can easily find that the target region contains gradual shades, which are not seen in the earlier images.

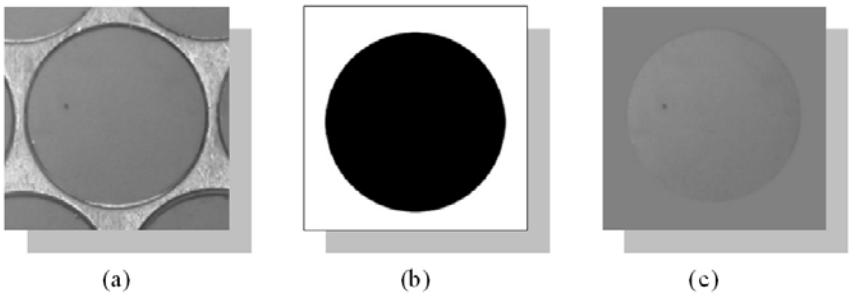

FIGURE 10. (a) Original testing image ($d_{x,y}$); (b) target mask image (IR_m); (c) mixed image ($d_{x,y}^{\#1}$) of capacitor chip

4.2. **Inspection performance in large sample size experiments.** The performance evaluation indices, $(1-\alpha)$ and $(1-\beta)$, are used to represent correct detection judgments;

the higher the two indices, the more accurate the detection results. Statistical type I error α suggests the probability of producing false alarms, i.e., detecting normal regions as flaws. Statistical type II error β implies the probability of producing missing alarms, which fail to alarm real flaws. We divide the area of normal region detected as flaws by the area of actual normal region to obtain type I error, and the area of undetected flaws by the area of actual flaws to obtain type II error. Therefore, the correct classification rate (CR) is defined as:

$$CR = (N_{cc} + N_{dd})/N_{total} \times 100\% \tag{18}$$

where N_{cc} is the pixel number of normal textures detected as normal areas, N_{dd} is the pixel number of flaws detected as defective regions, and N_{total} is the total pixel number of a testing image.

To demonstrate the flaw detection results, Figure 11 lists partial results of detecting slight surface variations by the Otsu method [22], the Iterative method [23], the Kapur's method [20], the proposed method, and the professional inspector, individually. The three spatial domain techniques, the Iterative, Otsu, and Kapur's methods, make lots of erroneous judgments (false alarms) on slight surface variation detection. The frequency domain technique, the proposed method, detects most of the slight surface variations and makes less erroneous judgments. Therefore, the frequency domain approach outperforms the spatial domain techniques in the slight surface variation detection of the capacitor chips.

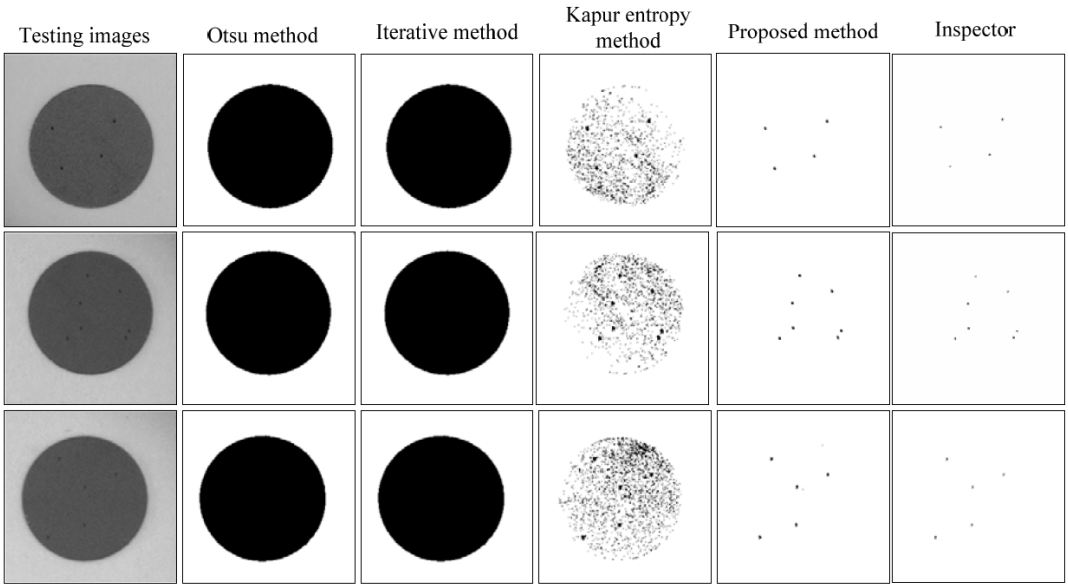

FIGURE 11. Partial detection results of the Otsu, Iterative, Kapur's entropy, the proposed methods, and inspector

To compare the performance of the slight surface variation detection, Table 1 summarizes the detection results of our experiments. The average defect detection rates $(1-\beta)$ of all testing samples by the four methods are, 99.99% (Otsu method), 99.99% (Iterative method), 98.74% (Kapur's method), and 96.66% (proposed method). However, the three spatial domain methods have significantly higher false alarm rates (α), 46.64% (Otsu method), 46.26% (Iterative method), and 10.34% (Kapur's method). On the contrary, the other frequency domain approach has rather lower false alarm rate, 0.12% (proposed method). The proposed method has higher correct classification rates (CR) than do the other methods applied to slight surface variation detection. The average computation

time for processing a testing image is as follows: 0.55 seconds by Otsu method, 0.62 seconds by Iterative method, 0.72 seconds by Kapur's method, and 2.48 seconds by proposed method. Hence, the proposed method can overcome the difficulties of detecting small defects and excel in its ability of correctly discriminating slight surface variations from normal regions.

TABLE 1. Summarized comparison table of slight surface variation detection of capacitor chips for four different methods

Methods	$1-\beta$ (%)	α (%)	CR (%)	Time (s)
Otsu method	99.99	46.64	54.26	0.55
Iterative method	99.99	46.26	54.73	0.62
Kapur's method	98.74	10.34	89.76	0.72
Proposed method	96.66	0.12	99.74	2.48

4.3. **Experiments on DCT reconstruction effects.** To evaluate the performance of the proposed DCT-based image reconstruction approach, experiments with and without the defect enhancement process are both conducted. The testing images with and without the DCT defect enhancement operation are all segmented by the Kapur's method to examine how they differ in terms of slight surface variation detection. Table 2 indicates the production related effects of slight surface variation detections by the current method, entropy method, and proposed method. Advantages of the proposed approach are summarized as follows:

(1) Both of the entropy and proposed methods excel in its ability of correctly discriminating slight surface variation blemishes from normal regions. The proposed method has lower false alarm rates and better detection rates than do the traditional methods.

(2) The two methods have higher correct classification rates than do the current human inspection method applied to slight surface variation detection of capacitor chip images.

(3) The proposed method has the lowest material wastage rate 1.6% and the smallest tolerance 2.2% of capacitor values compared with the current inspection method and entropy method due to the better blemish detection accuracy. The tolerance indicates how close the marked value of the capacitors is to its actual value. Cumulative slight surface variations cause a wide tolerance of capacitor values.

(4) The re-test rate for detecting slight surface variations of capacitor chips is as follows: 22.4% by the current method, 8.6% by the entropy method, and 1.8% by the proposed method. The re-test rate is the percentage of re-inspection and re-testing of chip products that have undergone rework or other modifications. The proposed method has respectively five times and twelve times lower average re-test rate than do the entropy method and the current method.

TABLE 2. The production related effects of slight surface variation detections by the three methods

Methods	Material wastage	Tolerance of capacitor values	Re-test rate
Human inspection (current method)	18.6%	8.8%	22.4%
Kapur's method	4.8%	5.4%	8.6%
Proposed method	1.6%	2.2%	1.8%

5. **Conclusions.** This paper presents a global approach for the automated visual inspection of slight surface variations in the surfaces of capacitor chips. Based on an image reconstruction scheme, it applies DCT disassembly and cumulative sum techniques to effectively detect slight surface variations. By analyzing the energy concentration condition of a chip frequency image, we can apply the DCT based approach to disassembling the frequency domain image into four disassembled matrices. From the disassembled odd-odd matrix, the cumulative sum algorithm can be used to select proper frequency values of large magnitude that represent the normal background texture of the chip surface. Then, we take out the selected frequency values of large magnitude and reconstruct the image from the DCT frequency matrix to remove the global random patterns of the statistically textured image and reserve local anomalies in the reconstructed image. Experimental results demonstrate that the proposed approach achieves high accuracy in detecting slight surface variations.

The processing time of the proposed approach can be significantly shortened after the parameter optimization is conducted and the DCT implemented in a single integrated circuit. If we do not count the time of taking forward and inverse DCT, the time of taking the RD-CUSUM method is less than 50 ms and the processing time of each method is very time-saving. The proposed method effectively and efficiently overcomes the difficulties of detecting small defects on capacitor chip images with random textured surfaces and excels in its ability of correctly discriminating slight surface variations from normal regions. Therefore, future research directions can focus on examining existing approaches to search for the most efficient and effective method for the proposed application.

Acknowledgement. This work was partially supported by the National Science Council (NSC) of Taiwan, under Grant No. NSC 100-2221-E-324-009-MY2.

REFERENCES

[1] H. D. Lin and Y. S. P. Chiu, RBF network and EPC method applied to automated process regulations for passive components dicing, *International Journal of Innovative Computing, Information and Control*, vol.6, no.11, pp.5077-5091, 2010.

[2] Z. Zhang, I. Nakamura, C. J. Li, T. Imamura, T. Miyake and H. Fujiwara, Metal plating surface defect detection by template matching using morphological processing, *ICIC Express Letters, Part B: Applications*, vol.2, no.3, pp.615-620, 2011.

[3] C. Y. Chang, C. H. Li, C. H. Chang and M. D. Jeng, Learning vector quantization neural networks for LED wafer defect inspection, *International Journal of Innovative Computing, Information and Control*, vol.4, no.10, pp.2565-2579, 2008.

[4] N. Araki, K. Nishiuchi, T. Sato, Y. Konishi, E. Fujiwara and H. Ishigaki, Defect detection for mirror polished metal surface using independent component analysis, *ICIC Express Letters*, vol.5, no.9(B), pp.3291-3295, 2011.

[5] W. C. Li and D. M. Tsai, Automatic saw-mark detection in multi-crystalline solar wafer images, *Solar Energy materials & Solar Cells*, vol.95, pp.2206-2220, 2011.

[6] Y. Han and P. Shi, An adaptive level-selecting wavelet transform for texture defect detection, *Image and Vision Computing*, vol.25, pp.1239-1248, 2007.

[7] H. D. Lin, Automated visual inspection of ripple defects using wavelet characteristics based multivariate statistical approach, *Image and Vision Computing*, vol.25, pp.1785-1801, 2007.

[8] X. Liu, Z. Wen, Z. Su and K. F. Choi, Slub extraction in woven fabric images using Gabor filters, *Textile Research Journal*, vol.78, no.4, pp.320-325, 2008.

[9] H. D. Lin and S. W. Chiu, Flaw detection of domed surfaces in LED packages by machine vision system, *Expert Systems with Applications*, vol.38, no.12, pp.15208-15216, 2011.

[10] A. Kumar, Computer-vision-based fabric defect detection: A survey, *IEEE Transactions on Industrial Electronics*, vol.55, no.1, pp.348-363, 2008.

[11] H. Y. T. Ngan, G. K. H. Pang and N. H. C. Yung, Automated fabric defect detection-a review, *Image and Vision Computing*, vol.29, pp.442-458, 2011.

[12] W. H. Chen, C. H. Smith and S. C. Fralick, A fast computational algorithm for the discrete cosine transform, *IEEE Transactions on Communications*, vol.25, no.9, pp.1004-1009, 1977.
[13] N. I. Cho and S. U. Lee, Fast algorithm and implementation of 2-D discrete cosine transform, *IEEE Transactions on Circuits and Systems*, vol.38, no.3, pp.297-305, 1991.
[14] R. C. Gonzalez and R. E. Woods, *Digital Image Processing*, 3rd Edition, Prentice Hall, New Jersey, USA, 2008.
[15] B. Chen, S. Latifi and J. Kanai, Edge enhancement of remote sensing image data in the DCT domain, *Image and Vision Computing*, vol.17, pp.913-921, 1999.
[16] Y. Zhong and A. K. Jain, Object localization using color, texture and shape, *Pattern Recognition*, vol.33, pp.671-684, 2000.
[17] C. W. Ngo, T. C. Pong and R. T. Chin, Exploiting image indexing techniques in DCT domain, *Pattern Recognition*, vol.34, pp.1841-1851, 2001.
[18] N. Ahmed, T. Natarajan and K. R. Rao, Discrete cosine transform, *IEEE Transactions on Computer*, vol.23, pp.90-93, 1974.
[19] D. C. Montgomery, *Statistical Quality Control: A Modern Introduction*, 6th Edition, John Wiley & Sons, New York, NY, USA, 2009.
[20] J. Kapur, P. Sahoo and A. Wang, A new method for gray-level picture thresholding using the entropy of the histogram, *Computer Vision, Graphics, and Image Processing*, vol.29, pp.273-285, 1985.
[21] M. Sezgin and B. Sankur, Survey over image thresholding techniques and quantitative performance evaluation, *Journal of Electronic Imaging*, vol.13, no.1, pp.146-165, 2004.
[22] N. Otsu, A threshold selection method from gray level histogram, *IEEE Transactions on Systems, Man and Cybernetics*, vol.9, pp.62-66, 1979.
[23] R. Jain, R. Kasturi and B. G. Schunck, *Machine Vision*, International Editions, McGraw Hill, New York, USA, 1995.